Intensity and phase fields behind phase-shifting masks studied with high-resolution interference microscopy

Krishnaparvathy Puthankovilakam
Toralf Scharf
Myun Sik Kim
Ali Naqavi
Hans Peter Herzig
Tina Weichelt
Uwe Zeitner
Uwe Vogler
Reinhard Voelkel

SPIE.

Intensity and phase fields behind phase-shifting masks studied with high-resolution interference microscopy

Krishnaparvathy Puthankovilakam,[a,*] Toralf Scharf,[a] Myun Sik Kim,[a] Ali Naqvi,[a] Hans Peter Herzig,[a] Tina Weichelt,[b] Uwe Zeitner,[b,c] Uwe Vogler,[d] and Reinhard Voelkel[d]
[a]Optics and Photonics Technology Laboratory, Ecole Polytechnique Fédérale de Lausanne, Rue de la Maladière 71b, CH-2002 Neuchâtel, Switzerland
[b]Friedrich-Schiller-Universität Jena, Institute of Applied Physics, Abbe Center of Photonics, D-07743 Jena, Germany
[c]Fraunhofer Institute for Applied Optics and Precision Engineering, D-07745 Jena, Germany
[d]SUSS MicroOptics SA, Rouges-Terres 61, 2068 Hauterive, Switzerland

Abstract. We try to find out the details of how light fields behind the structures of photomasks develop in order to determine the best conditions and designs for proximity printing. The parameters that we use approach real situations like structure printing at proximity gaps of 20 to 50 μm and structure sizes down to 2 μm. This is the first time that an experimental analysis of light propagation through a mask is presented in detail, which includes information on intensity and phase. We use high-resolution interference microscopy (HRIM) for the measurement. HRIM is a Mach–Zehnder interferometer, which is capable of recording three-dimensional distributions of intensity and phase with diffraction-limited resolution. Our characterization technique allows plotting the evolution of the desired light field, usually called the aerial image, and therefore gives access to the printable structure until the desired proximity gap. Here, we discuss in detail the evolution of intensity and phase fields of elbow or corner structures at different positions behind a phase mask and interpret the main parameters. Of particular interest are tolerances against proximity gap variation and the theoretical explanation of the resolution in printed structures. © *The Authors. Published by SPIE under a Creative Commons Attribution 3.0 Unported License. Distribution or reproduction of this work in whole or in part requires full attribution of the original publication, including its DOI.* [DOI: 10.1117/1.JMM.15.2.021203]

Keywords: proximity printing; phase-shifting mask; light evolution; high-resolution interference microscopy.

Paper 15168SSP received Nov. 2, 2015; accepted for publication Jan. 5, 2016; published online Jan. 29, 2016.

1 Introduction

In lithography, proximity printing is one of the oldest approaches to printing technology.[1–4] It is regarded as the most cost-effective printing technology for printing micrometer range structures. The resolution of the technology is limited due to the diffraction of light from the mask and corresponding propagation to the wafer. Therefore, the proximity gap between mask and wafer plays a major role in defining the properties of the printed structure in mask aligners. There are several resolution enhancement technologies (RETs) available to improve the resolution and quality of printing.[5–7] Some of them are: off-axis illumination, optical proximity correction (OPC), and a phase-shifting mask.[8–9] Among these, phase-shifting technology is one of the most prominent and efficient RETs with the disadvantage of much higher cost for the mask.[10] The success of phase-shifting technology is based on the possibility of creating high contrast by proper structuring of the materials. These shapes in the phase-shifting mask lead to the creation of phase singularities,[11] hence zones of zero intensity.

In this paper, we discuss phase-shifting mask structures and the propagation of light through them, with special emphasis on phase features. This is the first time that phase and intensity of an alternating phase-shifting mask have been evaluated, and aerial images are measured. There have been some earlier studies that describe aerial image formation and correction for the photomask. Such studies are mainly used for mask characterization and qualification.[12] There are also techniques for measuring the intensity of aerial images. However, those techniques and studies did not access the phase information. In our study, we focus on phase evolution from structures where some information exists that is available in phase-only images. The characterization and light field behind the mask are studied with high-resolution interference microscopy (HRIM).[13–14] HRIM is a Mach–Zehnder interferometer, which can measure three-dimensional (3-D) intensity and phase fields. The light evolution from the mask level of the structure to the wafer at a proximity gap of 50 μm is studied with HRIM. The aim of the study is to find the intensity and phase features of a phase-shifting mask at different proximity gaps. For our discussion and interpretation of results, we consider the concept of fractional Talbot images[15–17] that trigger the structure formation at different proximity gaps and for structures of only a few periods.

1.1 Structure

The intensity evolution of the light propagation from a binary mask having OPC structures for edge improvements has been tabulated earlier.[18] Here, the test structure is a group of corners or elbow structures from a phase-shifting mask.[19] Tina Weichelt (Friedrich-Schiller-Universität Jena) has developed the mask. The structure and details reported in Ref. 19 and the selected structure are shown in Fig. 1. The structure has a pitch of 4 μm and field size of 75×75 μm. The substrate material is fused silica (quartz), and the

*Address all correspondence to: Krishnaparvathy Puthankovilakam, E-mail: krishnaparvathy.puthankovilakam@epfl.ch
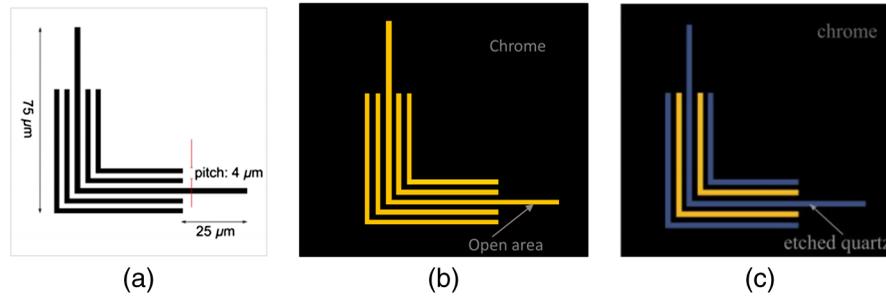
Fig. 1 Structure considered for our experiments, (a) the geometry of the structure, (b) amplitude structure (yellow lines are the open areas), and (c) the structure with phase shifts (yellow lines are the open areas and violet areas are the etched quartz) of π or a half wavelength.

structure is etched in such a way to get a phase shift of π or a half wavelength for the design wavelength, which was 365 nm. The smallest feature size is a 2-μm line, and the objective is to print the structure at a distance of 30 μm. As one can see in Fig. 1, one structure defines the geometry, one is the amplitude structure without phase change, and the last one is the phase structure where alternating phase between each corner structure is implemented.

1.2 High-Resolution Interference Microscopy: Experimental Setup

HRIM is a Mach–Zehnder interferometer, which can measure the light fields in 3-D. Figure 2 shows the basic layout of the HRIM interferometer system.

The type of source and the wavelength are decided according to the measurement problem. This might need to be highly coherent in case of phase measurements or have adjustable coherence for simulation of a real printing

situation. In the experiment presented here, we used a coherent monomode laser as the source. We used a stabilized monomode laser with coherence control from TOPTICA (TopMode CHARM) with a wavelength of 405 nm and 50 mW power to achieve a fully coherent illumination regime. The wavelength is close to those normally used in mask aligners and close to the design value. The laser beam will pass through an objective lens, which is spatially filtered by a pinhole and later expanded by a lens. The collimated beam will go through a beam splitter, splitting its path into the object arm and the reference arm.

The sample stage and the observation plane are in the object arm. A z-axis scanning piezo driver (closed loop operation—Mad City Labs Inc., Nano—Z500) in the object arm allows us to scan the sample along the propagation direction. Observation objective selection for the measurement has been done according to the sample size, the field size, and the correction of the objective for the wavelength. For the current measurements, we use a high-resolution
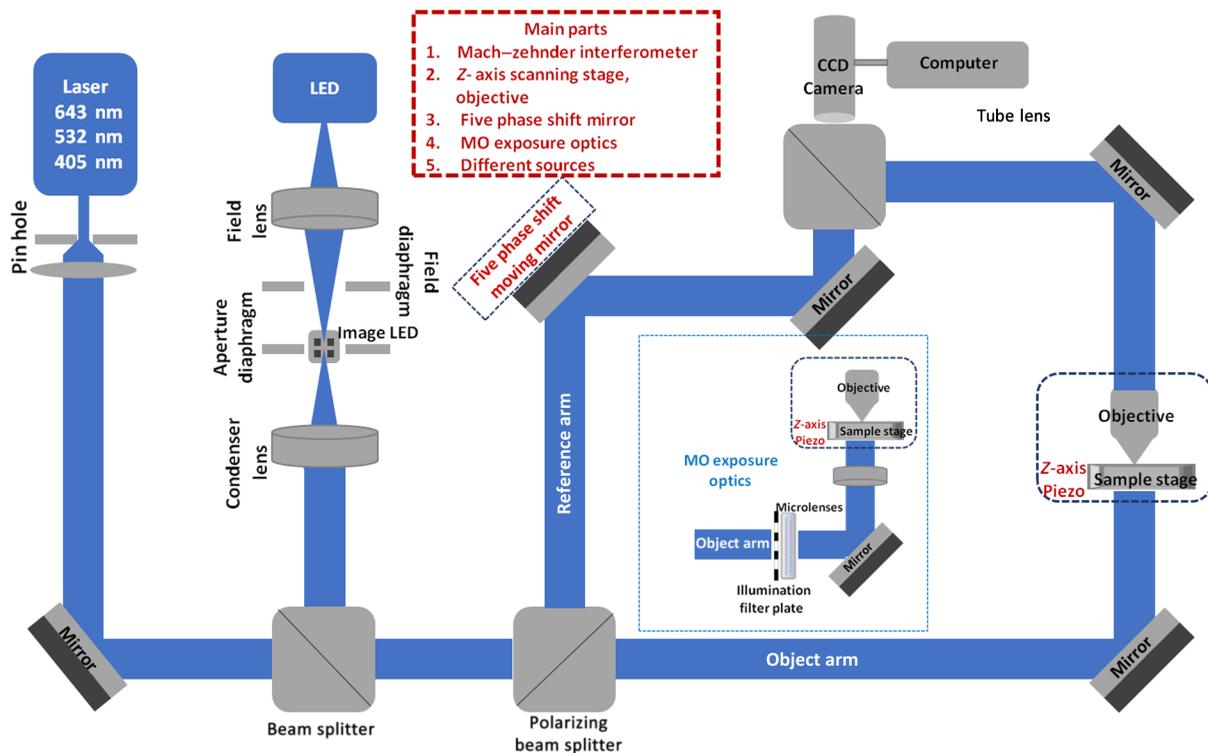
Fig. 2 The experimental setup—HRIM.

20 × /NA 0.75 dry objective (NIKON CFI Apochromat VC), corrected for 405 nm with the corresponding tube lens. The reference arm has a mirror mounted on the piezo actuator to allow phase shifting and a proper reconstruction of the measured phase. A beam splitter combines both beams from the object arm and reference arm, and the interferograms are recorded using a camera (charged-coupled device, Scion Corporation, CFW1312M camera with SONY ICX205AK image sensor of 1360×1024 pixels). The phase information is deduced by the five-phase shift algorithm using the movable mirror in the reference arm.[20]

2 Measurements and Recording

The main objective is to evaluate the light field behavior behind a normal amplitude mask and a phase-shifting mask. Figure 3 shows an intensity and phase image of the amplitude structure just above the mask. Figure 3(a) is the intensity image, and the phase image is plotted in Fig. 3(b). One recognizes the bright zones of light transmission in the functional structure and a stripe of high intensity to the left. Intensities are normalized to one. The phase image shows constant phase at openings indicated by uniform color. In zones without intensity beside the high-intensity zones, the phase could not be evaluated, which causes an undefined phase pattern.

Figure 4 represents an intensity and phase image of the phase-shifting mask structure just above the mask. As we mentioned, Fig. 4(a) represents the intensity, and phase is represented in Fig. 4(b). In Fig. 4 within the opening of the mask, one can clearly see the phase difference (π) between the open chromium and etched quartz in the corner structures with the color code: one part is red and the other part is blue. The phase images of Figs. 3 and 4 explain the phase differences between a normal amplitude mask and a phase mask structure. This type of phase image can also help to define the phase difference that we designed between etched quartz and the opening to verify the photomask.
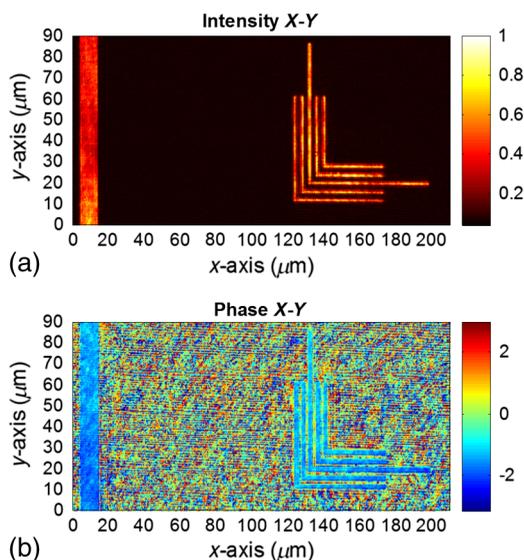
(a)

(b)
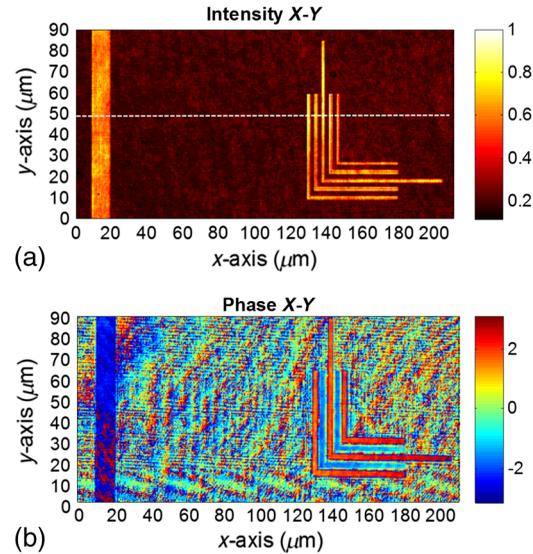
Fig. 4 (a) The measured intensity and (b) phase image of the phase-shifting mask structure at 0.1 μm proximity gap between the mask and observation plane. The intensities are normalized from 0 to 1, and phase values are from $-\pi$ (-3.14) radian to π (3.14) radian.

The phase measurements are done with a phase reference to make sure that the incident wave is a plane wave and the measurement is stable. As reference zones, we use the wide open areas in the field of view, which are far away from the measurement area, to ensure that the reference line does not influence the measurement. Here, the wide opening in the left side of Figs. 3 and 4 is the reference zone. The blue color refers to a certain phase level that is the same as the nonetched openings of the functional structures (Fig. 1).

The z-axis propagation is measured with the piezoelectric sample stage. This produces a huge volume of data when large area measurements are recorded at high precision. From that, we retrieve the propagation data from the line cuts of the desired area (the white dashed line on the intensity images of Figs. 3 and 4) and evaluate the light fields, their intensity, and phase.

2.1 Z–Axis Propagation Measurement

Propagation measurements mean the measurements along the propagation direction (in our case along the z-axis) and are done for a proximity gap of 50 μm.

2.1.1 Simulated light field study and propagation analysis

The first step is to verify the intensity light field with the help of simulation, to know the expected propagation result from an amplitude-only structure and the PSM structure necessary for comparison. The simulation software that we are using for studies is Layout LAB, specialized software for proximity, projection, and electron beam lithography in a single platform.[21] The software efficiently calculates the light propagation through the structures and gives the final resist model on wafers. The process window is designed by varying the exposure conditions, proximity gaps, and resist models. Proximity printing calculations are based on Rayleigh—Sommerfeld and the transfer matrix method. Here we are selecting two structures; one is amplitude only and other

(a)

(b)

Fig. 3 (a) The measured intensity and (b) phase image of the amplitude structure at 0.1 μm proximity gap between the mask and observation plane. The intensities are normalized from 0 to 1, and phase values are from $-\pi$ (-3.14) radian to π (3.14) radian.

is the phase-modulated structure, both with reference opening lines. If we make a line cut to get the propagation result, the structure will look like lines. Therefore, the selected structures for simulation are lines with same parameter conditions, which allow keeping the simulation one-dimensional (1-D).

Figure 5 shows the structures used for simulation in 1-D (line profile of phase and intensity). The amplitude structure is of lines with a width of 2 μm and a pitch of 4 μm. The phase structure has a phase difference between consecutive openings of half a design wavelength (π). The opening at the left is used as a reference. The width of the phase structure feature is 2 μm, and the period is 8 μm because the phase structure alternates, which leads to a doubling.

Figure 6 describes the evolution of light through the measured region of the structure at a position indicated by the white line in Fig. 3 until a proximity gap of 50 μm. The wavelength used for the simulation is 405 nm. A perfectly collimated (parallel) illumination is chosen in order to make sure that simulation and measurement conditions are as close as possible. A closer look reveals that the diffraction of light leads to varying intensity profiles at different proximity gaps as expected. We can observe that regions of highly confined light fields and diffraction effects are different for a normal amplitude mask and the phase mask. The diffraction effects also depend on Talbot length. For lithographic printing, several parameters are important: the contrast of the structure, the definition of the structure, and its position. The study will be complete only if we evaluate the propagation regions in more detail with the experimental result.

2.1.2 Experimental light field study using high-resolution interference microscopy and propagation analysis

Figure 7 shows the evolution of light through the measured region of the structure at a position indicated by the white line in Fig. 3. The light is coming from below, and the aerial images are recorded at different distances between mask and wafer with increasing distance of z from the mask. One recognizes that particular light bundles are visible in the intensity images that have a well-defined phase value. At zones with low intensity, for instance between 30 and 110 μm lateral positions (x-axis), the phase cannot be evaluated. We can define different interesting regions for printing and verify them by the intensity measurements for different zones of the proximity gap. In the regions until 20 μm of the proximity gap, all the lines are visible and good for printing. However, just after that, we can see the diffraction effects are prominent and lines are no longer differentiable. In

(a)

(b)

Fig. 6 The simulated light field propagation through (a) amplitude structure and (b) PSM structure for a proximity gap of 50 μm. Intensities are normalized to the maximum intensity.

(a)

(b)
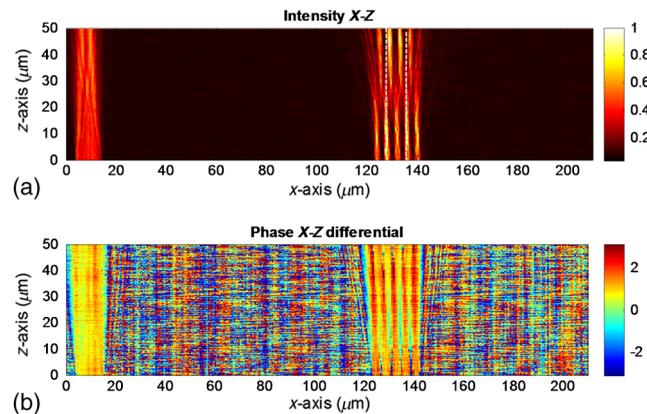
Fig. 7 (a) The measured intensity and (b) phase image of the light evolution for a proximity gap of 50 μm in amplitude structure. The intensities are normalized, and phase values are from $-\pi$ (-3.14) radian to π (3.14) radian.

the regions just above the diffraction regions, the contrast comes back for the lines. One counts only four intensity highs and sees a change of position shift. To guide the eye, white dashed lines are added in the intensity image of Fig. 7. Simulations of the amplitude structure in Fig. 6 also verify this change in features and positions. The position shift is explained by the Talbot effect, and further explanation is in Section 3.

To avoid the lateral shift and to print the correct structure on the exact positions of the mask, we need to use a

(a)

(b)

Fig. 5 The simulation structure. (a) Amplitude structure with 2 μm openings and 4 μm period. (b) The PSM structure of 2 μm openings and 8 μm period with phase changes similar to the measurement structure.
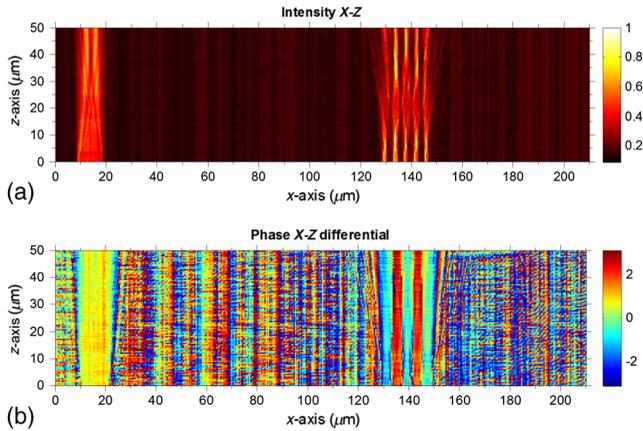
Fig. 8 (a) The measured intensity and (b) phase image of the light evolution for a proximity gap of 50 μm in phase-shifting mask structure. The intensities are normalized, and phase values are from $-\pi$ (−3.14) radian to π (3.14) radian.

phase-shifting mask. We will continue our discussion by focusing on the phase shift structure and the details of propagation of light through it. Figure 8 shows the propagation of light through the phase-shifting mask structure through the white dashed line region defined in Fig. 4.

Compared to Fig. 7, one can clearly notice the differences in intensity and phase patterns of Fig. 8. In intensity images, the high-contrast region after the diffraction effect appears at the same position and has the same high-intensity distribution exactly at the opening. The phase image clearly shows the phase difference between open chromium and etched quartz during the propagation of light and how it carries the information all along the propagation distance. Proximity printing relies on different factors like contrast and definition of intensity profile to define the aspect ratio of structures and resolution at different proximity gaps. To discuss the particularities of propagation, we take a closer look at the propagation measurement of intensity and

distinguish three zones along the propagation direction (z-axis). The first zone is just above the mask or the so-called contact region and reaches from mask level to a $\sim$10 μm proximity gap. Here, the structures have high contrast and all openings lead to intensity peaks. Printing in this region gives good results, but a small proximity gap carries the risk of touching the masks and damaging it—a known problem for contact printing. A second zone is defined between 10 and 32 μm, where one can clearly observe the washing-out of the well-defined intensity profile by diffraction effects. The contrast and shape of the structures are almost lost in this region, and printing would lead to unsatisfactory results. The structure could not be resolved even for severe conditions on dose and development (small process windows). The third zone extends just after this diffraction zone and ranges from 32 to 50 μm. In this zone, at some regions, the profile regains its properties, but usually with less contrast. The high-intensity lobes at the outer area are especially altered. To understand better what causes such behavior, we will evaluate all three regions more carefully with $x - y$ plane intensity and phase images. The theoretical explanation about different contrast effects and their positions in space is explained with the help of the Talbot effect.

2.2 $X - Y$ Image Plots and Line Plots

For evaluating the details about the exact intensity and phase profiles, we look at the $x - y$ plane images and line intensity plots at different proximity gaps. With this, we can make a better judgment on possible process windows, resolution, and structure fidelity. In Fig. 9, images are at a proximity gap of 5 μm, hence very close to the mask and in the first zone of interest.

Figure 9 represents the intensity and phase images of the $x - y$ plane and also the line intensity plots that have been averaged over several lines along the y-axis (35 to 55 μm) to increase the quality of the plot. The intensity image at the 5 μm proximity gap represents an ideal situation and
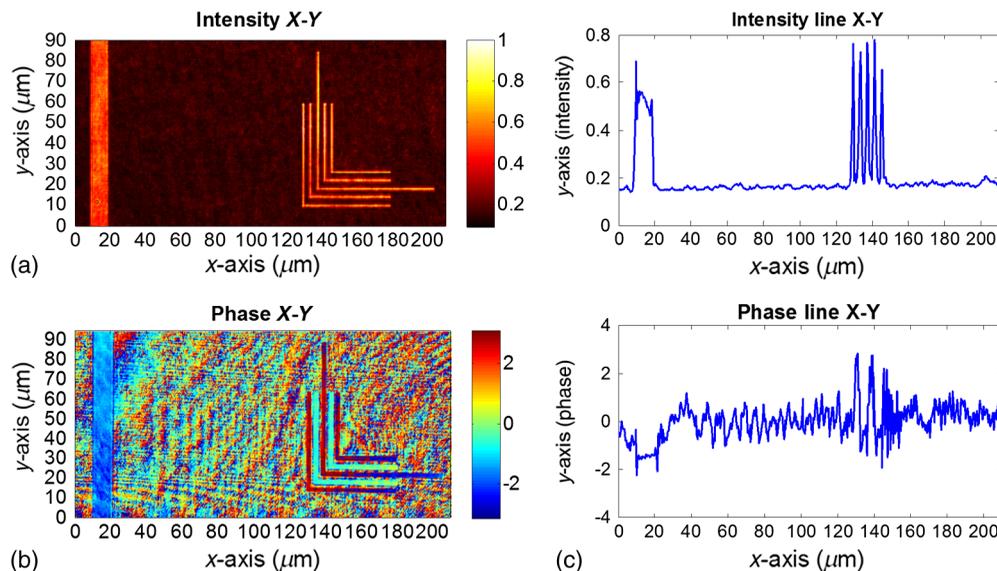
Fig. 9 (a) The measured intensity, (b) phase, and (c) line images of the phase-shifting mask structure at a 5 μm proximity gap. The intensities are normalized, and phase values are from $-\pi$ (−3.14) radian to π (3.14) radian.

shows all desired features of the structure, the five intensity maxima all with good contrast. The phase image represents a phase shift of π or a half wavelength between the etched quartz and open chromium at the designed position. The peaks in the line plots in Fig. 9 show very good agreement with the set phase shift of π within the precision of this measurement. Note that the design wavelength and our measurement wavelength differ slightly (365 versus 405 nm).

The second zone of interest is between 10 and 32 μm, where diffraction plays a major role. This zone is the typical working distance where standard mask aligners would deliver sufficient precision for positioning of the mask and wafer. Therefore, it is very interesting for technical applications.

Figure 10 gives the intensity and phase images at a gap of 22 μm behind the mask. From the intensity $x - y$ image, we clearly observe that the intensity does not show the design features anymore (compare with Fig. 4). The specific intensity profile of five peaks is lost, as well as the good contrast. The low-intensity regions between the multiple structures that are important for printing are washed out. Contrary to the intensity images, the phase images still show pronounced phase separation between zones, a phase change of π between adjacent zones. Such behavior indicates the existence of phase singularities. At the position of phase singularities, zero intensity is found, which is visible when comparing the intensities and phases in Fig. 10. What we observe here is that intensity zero regions are becoming very fine features and cannot be used for proper structure definition in printing. Because printing is based on intensity profiles, the region between 10 and 32 μm should be avoided for the geometry we consider here (feature size and period). The reason for this will be made clear by considering the Talbot effect, which is discussed later. It shall be noted that the creation of phase singularities with phase masks still keeps the information on the structure. Information with zero intensities is at the right position, but the contrast and intensity profiles cannot be used for printing anymore.
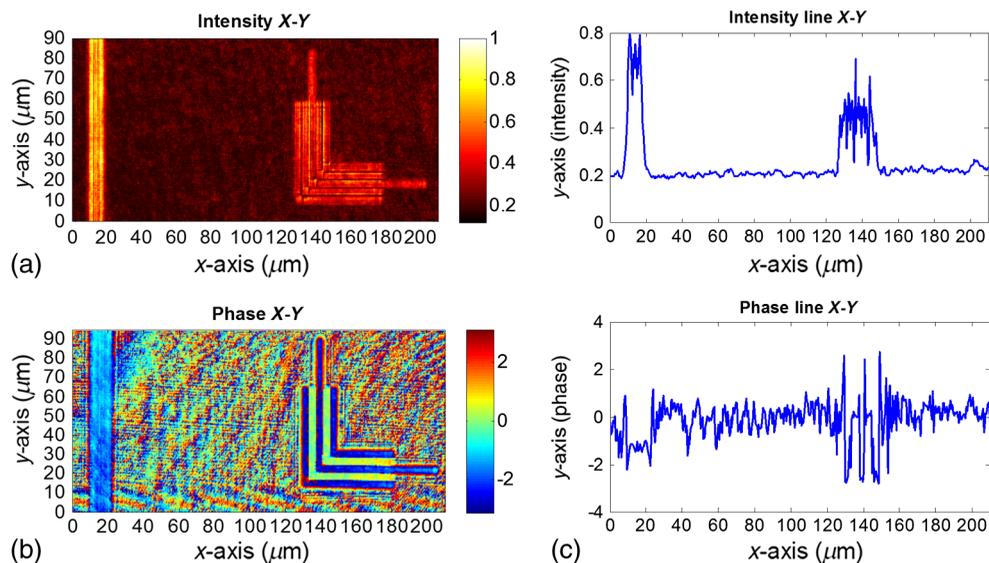
Surprisingly the situation changes when the light propagates further. We evaluate the measurement in the third zone of interest at a larger distance behind the mask from 40 to 50 μm. The result of the measurement is shown in Fig. 11. The intensity profile shows very good similarity with the desired one (compared to Fig. 4). The contrast is high and the intensity is low at the low-light zones. To see the effect of the alternating phase mask on a series of lines compared to a single structure, one can just examine the structure definition of a single line at the end of the corner structures in Fig. 11.

At the 40 μm proximity gap, the single line loses its definition completely, while the multiple corner structures can still be successfully printed and appear in good contrast. The $x - y$ intensity images show that the structure re-establishes the profile again, but lacks some of the original properties. The only difference is that the outward intensity peaks will have less intensity compared to the inner ones. This might lead to different line widths of outer and inner structures, but can be partially corrected using a particular dose setting or process window when printing.

3 Discussion

The experiments show propagation effects of light through an amplitude and a phase-shifting mask with repetitive features. Although we have only very few repetitions, interpretations can be made by assuming a periodic structure. When light falls on periodic structures such as gratings, Talbot images appear behind the structure. The Talbot effect structure is also valid for small grating periods.[22] The Talbot effect leads to varying light distribution and phase anomalies behind the grating.[23–25]

We can apply this concept to our case. The wavelength we are using for the measurement is 405 nm. For the amplitude-only mask structure with a period of $d = 4$ μm, one finds a Talbot distance $Z_{\mathrm{T}} = (2d^2/\lambda) = 79.01$ μm and a half Talbot distance of around 40 μm.[22] We know that at half Talbot distances, self-imaging occurs. These images are phase-shifted

Fig. 10 (a) The measured intensity, (b) phase and (c) line images of the phase-shifting mask structure at a 22 μm proximity gap. The intensities are normalized, and phase values are from $-\pi$ (-3.14) radian to π (3.14) radian.
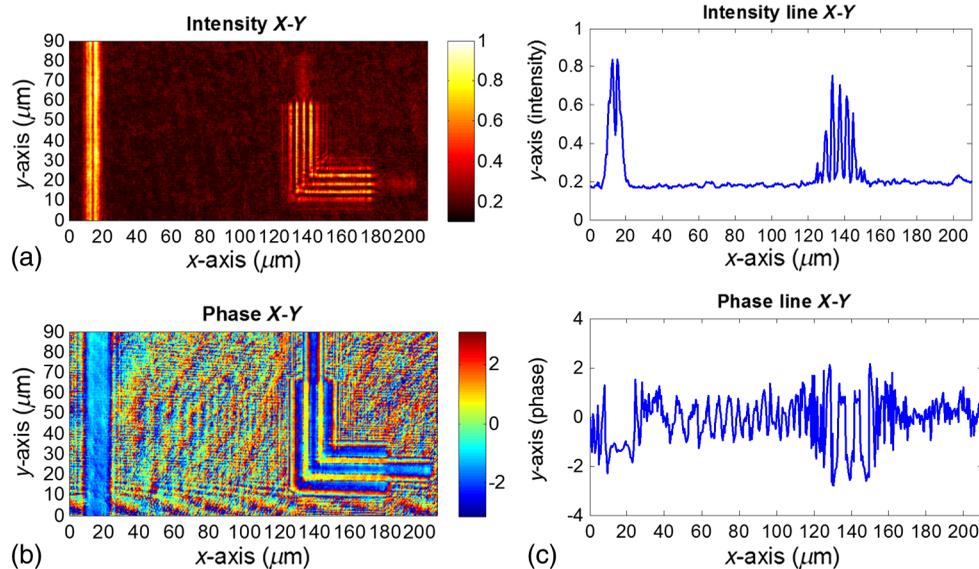
Fig. 11 (a) The measured intensity, (b) phase, and (c) line images of the phase-shifting mask structure at a 40 μm proximity gap. The intensities are normalized, and phase values are from $-\pi$ (-3.14) radian to π (3.14) radian.

by half a period, which means that the image position will be laterally shifting by half the width of the grating period. This corresponds to simulation and experimental findings of the high-contrast region at 40 μm distance behind the amplitude mask shown in Figs. 6(a) and 7.

A phase-shifting mask with base period $d = 8$ μm (the combination of amplitude and phase structures; compare with Fig. 1) will result in a Talbot distance of $Z_T = (2d^2/\lambda) = 316$ μm. This length is much longer than the distance range we are using for printing, which usually ranges only up to 50 μm. In one of the early papers, Lohmann pointed out that phase grating would form amplitude image copies at fractional Talbot distances.[16] This kind of imaging is only possible for certain phase-grating configurations, and the image formed is called a fractional Talbot image or Fresnel image. The Talbot distance depends not only on the period of the structure but also on the phase step.

In our case, the phase structure on the mask is neither a standard binary phase nor an amplitude-only grating. It is a complex structure having openings and phase shifts with a phase difference of π. According to Lohmann's interpretation, the new Talbot distance z can be linked to the original Talbot distance (Z_T) and numbers P and Q (where $P < Q$, and they are positive integers depending on the width of the structure w and period d). The fractional Talbot distance z becomes $z = (P/Q)Z_T$.

Self-imaging formed at different distances is explained according to the proper structuring of the mask. As discussed by Suleski,[17] a phase structure of π phase difference and a width-to-period ratio 1:4 will lead to a fractional Talbot image length (z) and Talbot length (Z_T) ratio of 1:8. If we apply this to our case, the width-to-period ratio is 1:4 (2/8) and the phase difference is π between etched quartz and open chromium. Then, the fractional Talbot image falls at a distance of $z = 1/8$th of $Z_T = 316$ μm/8 $= 40$ μm (approximately). This finding corresponds very well to the simulation and experimental findings of the high-contrast region at 40 μm distance behind the phase mask in Figs. 6(b) and 8. For distances below 40 μm, complex light patterns appear that cannot be optically resolved anymore with our measurement system. In printing, these zones will lead to nonuseful operation zones. An additional aspect is the limited number of periods. In such cases, the established pattern is washed out and contrast is reduced, which leads to an additional worsening of the pattern definition below the 40 μm distance limit.

4 Conclusion

We present phase and intensity profiles behind the mask structures in the proximity region upto 50 μm, (mask structures behind normal amplitude mask and structures in a phase-shifting mask). The results show how the phase encoding preserves the information when correctly applied. The above studies changed some ideas that existed until now in the printing industry, namely that shorter proximity gaps (but not contact) might give better results. It became clear that the proximity gap for printing a structure can be decided only after studying different parameters and conditions that are triggered by diffraction effects, measured by Fresnel numbers, and influenced by the resist properties. HRIM gives the opportunity to study the structure more deeply through intensity and phase profiles measured in 3-D, hence giving a full picture. The experimental evaluation of the structure at different proximity gaps allows us to understand the different effects. It also allows, in the longer run, optimization of printing as well as the development of rules of thumb for designing OPC structures.

References

1. J. H. Bruning, "Optical lithography-thirty years and three orders of magnitude: the evolution of optical lithography tools," *Proc. SPIE* **3051**, 14–27 (1997).
2. M. Rothschild et al., "Recents trends in optical lithography," *Lincoln Lab. J.* **14**(2), 221–236 (2003).
3. T. Ito and S. Okazaki, "Pushing the limits of lithography," *Nature* **406**, 1027–1031 (2000).
4. W. Henke et al., "Diffraction effects in submicron contact or proximity printing," *J. Microelectron. Eng.* **10**(2), 73–89 (1990).
5. A. K. Wong, *Resolution Enhancement Technologies in Optical Lithography*, SPIE Press, Bellingham, WA (2001).
6. F. M. Schellenberg, "A history of resolution enhancement technology," *Opt. Rev.* **12**(2), 83–89 (2005).
7. C. A. Mack, *Fundamental Principles of Optical Lithography: The Science of Microfabrication*, pp. 419–427, John Wiley & Sons, England (2007).
8. L. D. Huang and M. D. F. Wong, "Optical proximity correction (OPC): friendly maze routing," *Proc. DAC* **41**, 186–191 (2004).
9. M. D. Levenson, N. S. Viswanathan, and R. A. Simpson, "Improving resolution in photolithography with a phase-shifting mask," *IEEE Trans. Electron Devices* **29**(12), 1828–1836 (1982).
10. M. Fritze et al., "Subwavelength optical lithography with phase-shift photomasks," *Lincoln Lab. J.* **14**(2), 237–250 (2003).
11. M. D. Levenson, G. Di, and T. Ebihara, "The vortex mask: making 80 nm contacts with a twist!" *Proc. SPIE* **4889**, 1293–1303 (2002).
12. A. Garetto, T. Scherübl, and J. H. Peters, "Aerial imaging technology for photomask qualification—from a microscope to a metrology tool," *Adv. Opt. Technol.* **1**(4), 289–298 (2012).
13. M. S. Kim, T. Scharf, and H. P. Herzig, "Small-size microlens characterization by multiwavelength high-resolution interference microscopy," *Opt. Express* **18** (14), 14319–14329 (2010).
14. T. Scharf, M. S. Kim, and H. P. Herzig, "Measuring amplitude and phase of light emerging from microstructures with HRIM," *Proc. SPIE* **8082**, 101–108 (2011).
15. M. V. Berry and S. Klein, "Integer, fractional and fractal Talbot effects," *J. Mod. Opt.* **43**(10), 2139–2164 (1996).
16. A. W. Lohmann and J. A. Thomas, "Making an array illuminator based on the Talbot effect," *Appl. Opt.* **29**(29), 4337–4340 (1990).
17. T. J. Suleski, "Generation of Lohmann images from binary-phase Talbot array illuminators," *Appl. Opt.* **36**(20), 4686–4691 (1997).
18. K. Puthankovilakam et al., "Shaping intensity behind amplitude masks for proximity correction lithography: design, measurement and realization," *Proc. SPIE* **9203**, 92031B (2014).
19. T. Weichelt et al., "Resolution enhancement for advanced mask aligner lithography using phase-shifting photomasks," *Opt. Express* **22**(13), 16310–16321 (2014).
20. P. Hariharan, B. F. Oreb, and T. Eiju, "Digital phase-shifting interferometry: a simple error-compensating phase calculation algorithm," *Appl. Opt.* **26**(13), 2504–2506 (1987).
21. A. Bramati et al., "Simulation tools for advanced mask aligner lithography," *Proc. SPIE* **8167**, 81670U (2011).
22. M. S. Kim et al., "Talbot images of wavelength scale amplitude gratings," *Opt. Express* **20**(5), 4903–4920 (2012).
23. M. S Kim et al., "Phase anomalies in Talbot light carpets of self-images," *Opt. Express* **21**(1), 1287–1300 (2013).
24. H. H. Solak, C. Dais, and F. Clube, "Displacement Talbot lithography: a new method for high-resolution patterning of large areas," *Opt. Express* **19**(11), 10686–10691 (2011).
25. H. H. Solak et al., "Phase shifting masks in displacement Talbot lithography for printing nano-grids and periodic motifs," *Microelectron. Eng.* **143**, 74–80 (2015).

Krishnaparvathy Puthankovilakam is a doctoral student in the Optics and Photonics Technology Laboratory, Ecole Polytechnique Fédérale de Lausanne, Switzerland. She received her MSc (Tech) degree in photonics from the National Institute of Technology Calicut, India, in 2012.

Biographies for the other authors are not available.